Journal of Hepatocellular Carcinoma

Dovepress

open access to scientific and medical research

Open Access Full Text Article

ORIGINAL RESEARCH

Quantitative Assessment of Hypovascular Component in Arterial Phase to Help the Discrimination of Combined Hepatocellular-Cholangiocarcinoma and Hepatocellular Carcinoma

Xue Yang[1,*], Jing Chang[2,*], Ruili Li[3], Yu Qi[1], Xufen Zeng[4], Wei Wang[1], Hongjun Li[1]

[1]Department of Radiology, Beijing YouAn Hospital, Capital Medical University, Beijing, 100069, People's Republic of China; [2]Department of Pathology, Beijing YouAn Hospital, Capital Medical University, Beijing, 100069, People's Republic of China; [3]Department of Radiology, Xuanwu Hospital Capital Medical University, Beijing, 100073, People's Republic of China; [4]Department of Nutrition, School of Public Health, Anhui Medical University, Hefei, Anhui, 230032, People's Republic of China

*These authors contributed equally to this work

Correspondence: Hongjun Li, Department of Radiology, Beijing YouAn Hospital, Capital Medical University, No. 8 Xi Tou Tiao, Youanmen Wai, Fengtai District, Beijing, 100069, People's Republic of China, Email lihongjun00113@ccmu.edu.cn

Purpose: To explore the imaging performance for discrimination of combined hepatocellular- cholangiocarcinoma (cHCC-CCA) and hepatocellular carcinoma (HCC).

Methods: In total, 35 patients with cHCC-CCA and a matched control group of HCC patients (n = 35) were included retrospectively. We quantitatively evaluated the hypovascular component in tumor and qualitatively assessed LI-RADS features and other aggressive features to develop model for cHCC-CCA diagnose. Subgroup analyses were performed by tumor size and LI-RADS category.

Results: cHCC-CCA frequently showed a larger proportion (≥50%) of hypovascular areas followed by HCC (P = 0.000). Among those patients with ≥50% hypovascular areas, 8 patients did not present rim enhancement in atrial phase. The LI-RADS major features were more commonly observed in HCC (82.9–45.7%,), than cHCC-CCA (*P* = 0.003–0.022). The targetoid appearances and non-smooth margin frequently appeared in cHCC-CCA (34.3–63.9%), compared with HCC (*P* = 0.000–0.023). We developed a radiologic model based on ≥50% hypovascular component and delayed enhancement, which presented AUC of 0.821, accuracy of 80%. We also obtained good performance by radiologic model in LR-M group and tumor size <50mm group (AUC: 0.841 and 0.866, respectively). Combined group which included CA 19–9 and ≥50% hypovascular component and delayed enhancement did not improve the distinction performance between cHCC-CCA and HCC, which presented good performance of identifying cHCC-CCA in the LR-4/5 subgroup and tumor size ≥50 mm subgroup (AUC: 0.717, 0.730, respectively). cHCC-CCA group presented heterogeneous dominant pathology involving 15 of HCC, 7 of intrahepatic cholangiocarcinoma (iCCA) or cholangiolocellular carcinoma (CLC), 13 of intermediate cells component. Macrotrabecular appearances were higher in cHCC-CCA than that in HCC. The proportion of Hepa-1 was significantly higher in true negative (TN) patients (29 [93.5%]) and false negative (FN) patients (10 [100%]) than in true positive (TP) patients (16 [64%]; *P* = 0.036).

Conclusion: Quantitative assessment of hypovascular component could help the discrimination of cHCC-CCA. Macrotrabecular appearances were more exhibited in cHCC-CCA than that in HCC.

Keywords: combined hepatocellular-cholangiocarcinoma, hepatocellular carcinoma, computed tomography, magnetic resonance imaging, pathologic feature, cHCC-CCA, HCC, CT

Received: 30 September 2022
Accepted: 10 December 2022
Published: 26 January 2023

Introduction

Combined hepatocellular-cholangiocarcinoma (cHCC-CCA) is the rare form of primary liver cancer, accounting for only 0.4–14.2% of all cases.[1] The trend of cHCC-CCA for prognosis is generally to be worse than that of hepatocellular carcinoma (HCC).[2] Furthermore, the appropriateness of treatment is different from classic HCC, especially concerning liver transplantation.[3] In this respect, it is of high clinical value in differentiating cHCC-CCA from HCC. The newest edition of the World Health Organization's (WHO) classification (2019) recommends that cHCC-CCA includes all of the combined tumor components, such as cHCC-CCA, cHCC-cholangiolocellular carcinoma (CLC), cHCC-CCA-CLC, and cHCC-CCA-intermediate cells carcinoma. Because of the complexity of the pathology, cHCC-CCA could present heterogeneous appearance. cHCC-CCA is also predominant in patients with the overlapping risk factors of HCC. Those features add the difficulty of distinguishing it from HCC.[4]

The Liver Imaging Reporting and Data System (LI-RADS) is a standardized system based on the summary of various imaging appearances.[5,6] Previous studies reported that LR-5 category presented a sensitivity of 69% and a specificity of 87% about HCC identification. The false-positive diagnoses mainly derived from the misclassification of cHCC-CCA.[7] Jeon et al demonstrated that patients with 10% LR-M category were diagnosed as having HCC.[8] LR-M category is considered as very likely to be a malignant lesion, a biopsy is recommended for a correct diagnosis.[9] Regarding the biopsy's potential complications and costs, as well as corresponding selection bias due to high tumor heterogeneity, diagnosis of cHCC-CCA is still considered as a dilemma. Enhancement was associated with a larger area of the HCC component, smaller CC component, and less fibrotic stroma.[2] Some studies have explored the power of imaging features to distinct cHCC-CCA and HCC. They presented part discordance when identifying cHCC-CCA from HCC using imaging features.[10–14] Gigante et al demonstrated a mixed enhancement pattern provided high specificity for cHCC-CCA diagnosis (81%),[10] whereas Shin et al and Le et al showed rim APHE or targetoid appearances, not mix pattern, was the highest frequency in non-HCC malignancies.[11,14] Thus, more studies were required to be further explored to improve the distinction cHCC-CCA from HCC. The hypointense in arterial phase (AP) was mainly considered as the imaging appearances of hypoxic and fibrotic micro-environments in tumor, which was also associated with aggressive characteristics.[15,16] Regarding poor prognosis of cHCC-CCA, the proportion of hypointense in the AP may help improving the discrimination of cHCC-CCA and HCC.

Additionally, some CT findings, including intratumoral artery, non-smooth tumor margin may also serve as the aggressive features of HCC.[17,18] It is plausible to assume that cHCC-CCA may be distinguishable applying those findings related to aggressive behavior.

The purpose of our study was to determine imaging features bearing aggressive nature in the differentiation of cHCC-CCA from HCC, and its capability of pathology indication.

Material and Methods Study Population

This single-center study consisted of 35 consecutive patients with cHCC-CCA from January 1, 2013, to December 31, 2021. This retrospective research only contained some existing data from the medical records of patients which was used to statistical analysis. At the process of analysis, all of data was anonymous and did not include the privacy information. And there is not any behavior that is detrimental to the patient’s health. The research covered patient data confidentiality. Based on all characteristics of the research, it was performed in accordance with the ethical guidelines of the Declaration of Helsinki and approved by the ethical committees of the Beijing Youan Hospital, Capital Medical University.

Histopathologic diagnosis of cHCC-CCA was reevaluated consistent with the 2019 World Health Organization Histological Classification System.[19] The requirement for patient consent was waived. Following inclusion criterion were used: 1) initially curative surgery resection of tumor with postoperative pathology; 2) the enhanced computed tomography (CT) or/and magnetic resonance imaging (MRI) examinations performed within 1 month before surgery. Patients were excluded if they were: 1) only diagnosed by biopsy pathology; 2) underwent other preoperative treatment. Additionally, we included 35 patients with surgically identified HCC to comparison. Those patients were in accordance with above inclusion and exclusion criteria and separately selected through 1:1 matching with cHCC-CCA based on age, tumor size, tumor number, Child-Pugh classification (match tolerance:0.02). A flow chart for population is provided in Figure 1.

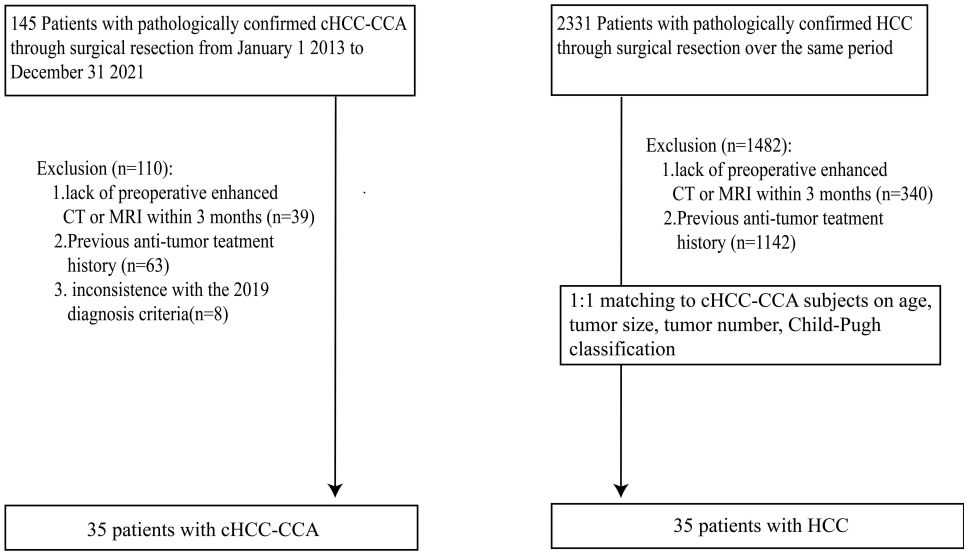

Figure 1 Flowchart demonstrating recruitment pathway for the population.
Abbreviations: cHCC-CCA, combined hepatocellular- cholangiocarcinoma; HCC, hepatocellular carcinoma; CT, computed tomography; MRI, magnetic resonance imaging.

Measurement of Clinical and Pathological Data

Clinical information and laboratory data were collected including patients' demographics, etiology, Child-Pugh classification, serum biochemicals and tumor biomarker within 7 days before curative resection. Since carbohydrate antigen-199 (CA19-9) was missing in 4 patients, median was considered as the replacement.

Two pathologists reevaluated the histopathological images of cHCC-CCA with immunohistochemical results, which also delineated the dominant pathology, hepatocyte-1 (Hepa- 1), glypican-3 (GPC-3), cytokeratin-7 (CK7), CK19. The whole tumor was dissected if tumor size was smaller than 20mm, otherwise sagittal and coronal sections with maximum diameter were selected, to assure the accuracy of pathological diagnosis.

Imaging Protocol and Analysis

Overall, 80% (n = 56) of patients were imaged with enhanced CT (cHCC-CCA: 27, HCC: 29), and 37.14% patients were imaged using enhanced MRI (cHCC-CCA: 12, HCC: 14).

Contrast-enhanced CT scanning protocol was summarized in the Supplemental Table 1. The MRI with contrast agents protocol was presented in Supplemental Table 2.

Two faculty abdominal radiologist with 5–10 years' experience independently reviewed the CT/MRI images, who blinded to other data. When the patient had multiple tumors, reviewers chose the largest one. Reviewers reported the proportion of hypovascular component. Other image appearances were also evaluated: tumor size, tumor margin, intratumoral artery, LI-RADS category based on LI- RADS v2018[20] (definition shown in Supplemental Table 3 in details). Parts of ancillary imaging features and targetoid appearance were evaluated through MRI imaging including marked diffusion restriction, and mild-moderate T2 hyperintensity, and TP hypointensity, and fat in mass more than adjacent liver, and targetoid TP appearance, and targetoid diffusion restriction. Other imaging features were assessed via combination of two imaging approaches when the subject underwent CT and MRI, otherwise only by single one approach.

Statistical Analysis

Statistical analysis was produced by SPSS software ver. 26.0. Continuous data was evaluated differences using Student's *t*-test if data was in accordance with normal distribution and homogeneity of variance, otherwise by Mann–Whitney *U*-test. Differences about frequencies of categorical variables were assessed using χ^2 test. When expected count ranged from 1 to 5, Continuity Correction was applied. Moreover, variables were analyzed through Fisher exact test, whose expected counts were lower than 1. Pearson χ^2 test could be used to comparing other variables which were larger than 5.

In order to minimize the model over-fitting risk, we excluded imaging features which only evaluated through enhanced MRI holding too low frequent prevalence. Univariate and multivariable logistic regression analysis were performed to determine factors associated with cHCC-CCA. Performances of the diagnostic models for cHCC-CCA were evaluated using area under the receiver operating curve (AUC), 95% confidence intervals (CIs), sensitivity, specificity, and accuracy. Subgroup analyses were performed based on tumor size and LI-RADS category. Interreader agreement among three observers for imaging features was assessed by Kappa value (Supplemental Table 4).

Results

Clinico-Pathological Characteristics of cHCC-CCA and HCC

The outcome included 70 patients (56 (80%) males and 14 (20%) females) with a median age of 55 years (ranges from 50–60 years). Table 1 displays detailed clinico-pathological results of those patients. Some clinico-pathological features had

Table 1 Comparison of Clinico-Pathological Features Between cHCC-CCA and HCC

Variable	cHCC-CCA (n = 35)	HCC (n = 35)	*P* value
Clinical findings			
Age(years)	54.2±8.156	52.86±11.39	0.323
Gender (Male [%])	26 (74.3%)	30 (85.7%)	0.232
Etiology (%)			
None	5 (14.3%)	1 (2.9%)	0.289
HBV	28 (80%)	32 (91.4%)	
HCV	2 (5.7%)	2 (5.7%)	
Child-Pugh classification (A [(%])	33 (94.3%)	33 (94.3%)	1.000
Cirrhosis (%)	17 (48.6%)	18 (51.4%)	0.811
AFP (>20 ng/mL [%])	15 (42.9%)	16 (45.7%)	0.810
CA19-9 (>37 U/mL [%])	13 (37.1%)	4 (11.4%)	0.012*
ALT (U/L)	22 (19–38)	26 (19–39)	0.335
AST (U/L)	26 (21–37)	26 (22–35)	0.698
TBIL (umol/L)	14.6 (11.3–22.9)	15.7 (13–20.2)	0.545
DBIL (umol/L)	4.6 (3.4–7.1)	5.2 (4.1–7.1)	0.381
Albumin (g/l)	41.66±3.88	40.84±4.92	0.144
GGT (U/L)	39.5 (25–62)	30 (20–49)	0.298
PT (sec)	11.7 (11.1–12.5)	12 (11.5–12.9)	0.111
PLT (*10^9 /L)	164 (116–224)	152 (118–219)	0.283
Pathological features			
Tumor number (%)	33 (94.3%)	34 (97.1%)	1.000
Tumor size (≥50mm [%])	15 (42.9%)	7 (20%)	0.070
Tumor necrosis	14 (40%)	10 (28.6%)	0.314
Vascular invasion (%)	16 (45.7%)	19 (54.3%)	0.631
MVI (%)	18 (51.4%)	20 (57.1%)	0.631
Macrovascular invasion (%)	2 (5.7%)	3 (8.6%)	1.000
Satellite nodules (%)	13 (37.1%)	5 (14.3%)	0.029*
Macrotrabecular appearance	9 (25.71%)	2 (5.71%)	0.022*
CK19	30 (85.7%)	6 (17.1%)	0.000*
Hepa-1	26 (74.3%)	33 (94.3%)	0.022*
GPC-3	26 (74.3%)	29 (82.9%)	0.382
CK7	29 (82.9%)	9 (25.7%)	0.000*

Notes: According to whether the data conforms to the normal distribution, continuous variables are presented as median (range) or mean±standard deviation and analyzed using independent *t*-test or Mann–Whitney *U*-test. Categorical variables are expressed by number and percentage and compared by Pearson's χ^2 test or Continuity Correction or Fisher's exact test. *$p<0.05$.
Abbreviations: cHCC-CCA, combined hepatocellular- cholangiocarcinoma; HCC, hepatocellular carcinoma; HBV, hepatitis B virus; HCV,hepatitis C virus; AFP, alpha-fetoprotein; CA19-9, carbohydrate antigen-199; ALT, alanine aminotransferase; AST, aspartate aminotrans ferase; TBIL, total bilirubin; DBIL, direct bilirubin; GGT, gamma-glutamyltransferase; PT, prothrombin time; PLT, platelet count; MVI, microvascular invasion; CK19, cytokeratin-19; GPC-3, glypican-3; CK7, cytokeratin-7.

significantly difference between cHCC-CCA and HCC, including macrotrabecular appearance, serum CA19-9, satellite nodules, hepatocyte-1 (Hepa-1), cytokeratin-7 (CK7), CK19 (P = 0.000–0.022, < 0.05). In cHCC-CCA, tumors with macrotrabecular appearance derived from hepatocyte or intermediate cells (Figure 2). cHCC-CCA group presented heterogeneous dominant pathology involving 15 (42.86%) of HCC, 7 (20%) of iCCA or CLC, 13 (37.14%) of intermediate cells component.

Imaging Findings Between cHCC-CCA and HCC

cHCC-CCA frequently showed larger proportion (≥50%) hypovascular areas followed by HCC (P = 0.000). Among those patients with≥50% hypovascular areas, 8 patients did not present rim enhancement in atrial phase. The detailed radiological features of two groups were summarized in Table 2. LI-RADS category was different between cHCC-CCA and HCC (LR-M: 22 [62.9%] vs. 5 ([14.3%], LR-4/5: 10 [28.57%] vs. 29 [82.56%]). Additionally, in cHCC-CCA group, 25.7% was designated as LR-5, that is to say, those lesions took false positive (FP) diagnoses as HCC. The LI- RADS major features were more commonly observed in HCC (82.9–45.7%,), than cHCC-CCA (*P* = 0.003–0.022,<0.05). The targetoid appearances and non-smooth margin frequently appeared in cHCC-CCA (34.3–63.9%), compared with HCC (*P* = 0.000–0.023,<0.05).

Performance of Diagnostic Models for cHCC-CCA

According to univariate regression, CA19-9, ≥50% hypovascular component, and tumor margin, and LI-RADS major features, LI-RADS targetoid appearances were associated with cHCC-CCA (Table 3).

By multivariate regression analyses, ≥ 50% hypovascular component and delayed central enhancement showed strong association with cHCC-CCA (OR [95% CI]): 10.873 (2.549–46.391) (P = 0.001), OR (95% CI): 14.242 (1.561–129.917) (*P* = 0.009) (Table 3). When radiologic model with ≥50% hypovascular component and delayed central enhancement was considered as the diagnosis criteria, the better AUC of 0.821, and better accuracy of 80%, and higher sensitivity of 71.43%, and higher specificity of 88.57% were obtained than LR-M (AUC, accuracy and specificity: 0.743, 72.86%,

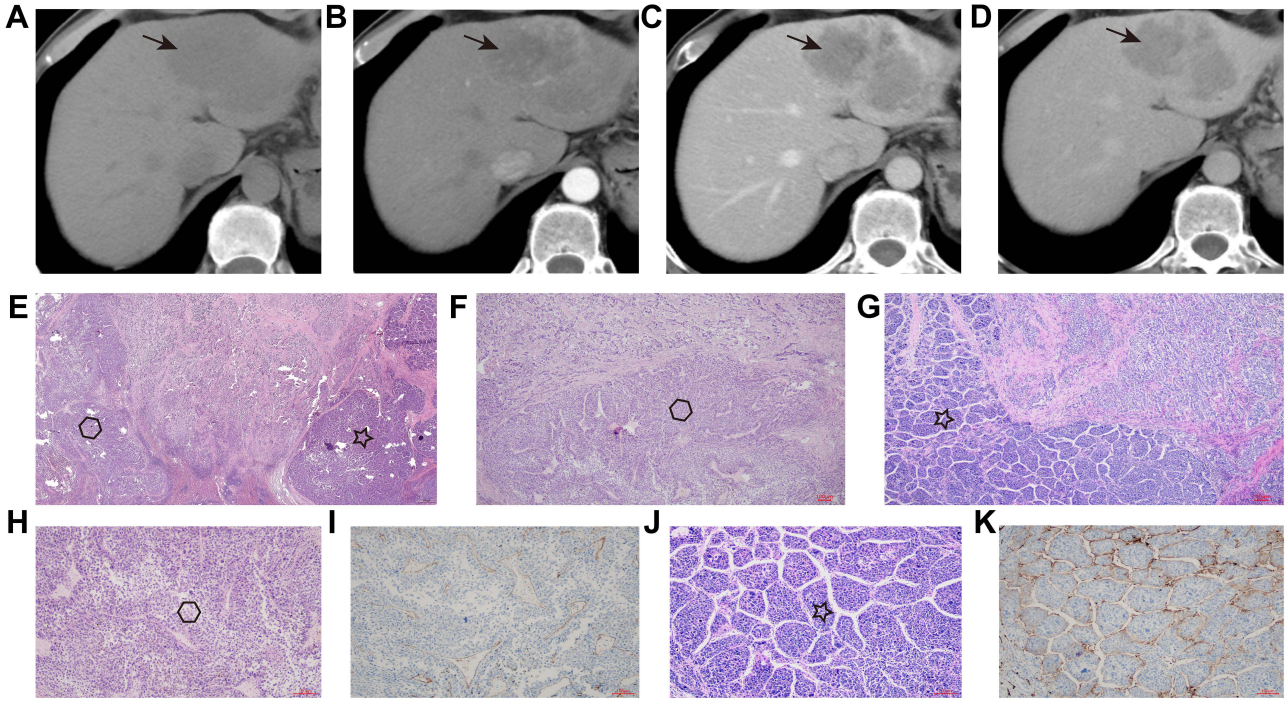

Figure 2 Example of a patient with tumor cells arranged by macrotrabecular or macrotrabecular-massive appearance (cHCC-CLC-Intermediate cells subtype). (**A**–**D**). contrast- enhanced CT images. (**E**–**H** and **J**). Hematein and Eosin staining. (**F** and **H**). macrotrabecular-massive permutation (⬡), (**G** and **J**). vessels that encapsulate tumor clusters (VETC) pattern (☆). (**I** and **K**). present outcome of CK34 in those two arrangements.

Table 2 The Results of Imaging Characteristics with Enhanced CT or MRI Between cHCC-CCA and HCC

Variable	cHCC-CCA (n = 35)	HCC (n = 35)	*P* value
Hypovascular component (≥50% [%])	22 (62.9%)	3 (8.6%)	0.000*
Internal arteries (%)	17 (48.6%)	16 (45.7%)	0.811
Tumor margin (smooth [%])	13 (37.1%)	23 (65.7%)	0.017*
LI-RADS category (%)			0.000*
LR-M	22 (62.9%)	5 (14.3%)	
LR-TIV	3 (8.6%)	1 (2.9%)	
LR-5	9 (25.7%)	28 (80%)	
LR-4	1 (2.9%)	1 (2.9%)	
Major imaging features			
Non-rim like enhancement in AP (%)	17 (48.6%)	29 (82.9%)	0.003*
Non-peripheral "washout"in PVP or DP/TP (%)	17 (48.6%)	29 (82.9%)	0.003*
Enhancing capsule (%)	7 (20%)	16 (45.7%)	0.022*
Ancillary imaging features			
Corona enhancement (%)	4 (11.7%)	3 (8.8%)	1.000
Marked diffusion restriction (%)†	8/12 (66.7%)	6/14 (42.9%)	0.225
Mild-moderate T2 hyperintensity (%)†	12/12 (100%)	13/14 (92.9%)	1.000
TP hypointensity (%)†	5/12 (41.7%)	13/14 (92.9%)	0.009*
Non-enhancing capsule (%)	0	1 (2.9%)	1.000
Nodule-in-nodule (%)	0	1 (2.9%)	1.000
Mosaic architecture (%)	7 (20%)	8 (22.9%)	0.771
Fat in mass, more than adjacent liver (%)†	2/12 (16.7%)	1/14 (7%)	0.580
Blood products in mass (%)	4(11.4%)	6(17.1%)	0.495
Targetoid mass, imaging appearance			
Rim arterial phase hyperenhancement (%)	18 (51.4%)	5 (14.3%)	0.001*
Peripheral "washout" in PVP or DP/TP (%)	12 (34.3%)	4 (11.4%)	0.023*
Delayed central enhancement (%)	16 (45.7%)	1 (2.9%)	0.000*
Targetoid TP appearance (%)†	2/12 (16.7%)	0	0.203
Targetoid diffusion restriction (%)†	1/12 (8.3%)	0	0.462
Biliary dilatation (%)	4 (11.4%)	1 (2.9%)	0.356
Lymph node invasion (%)	3 (8.6%)	1 (2.9%)	0.614
Liver capsular retraction (%)	5 (14.3%)	2 (5.7%)	0.428

Notes: †Data are numbers of patients who were evaluated by MRI. Categorical variables are expressed by number and percentage. *P<0.05.

Abbreviations: cHCC-CCA, combined hepatocellular- cholangiocarcinoma; HCC, hepatocellular carcinoma; CT, computed tomography; MRI, magnetic resonance imaging; LI-RADS, Liver Imaging Reporting and Data System; LR- TIV, LR tumor in vein; AP, arterial phase; PVP, portal vein phase; DP, delayed phase; TP, transitional phase.

62.86%, and 85.71%, respectively). As combined with CA19-9 (combined model), accuracy, and sensitivity, and specificity have not improved any more (Table 4).

Furthermore, regarding to difference LI-RADS category between cHCC-CCA and HCC, we also conducted subgroup analysis. Combined model presented high accuracy and specificity in LR-4/5 group. In LR-M group, we obtained high accuracy and sensitivity by both radiologic model and combined model.

The hypovascular component may be effected by tumor size which prone to tumor necrosis. Thus, we performed subgroup analysis to test the diagnostic value according to tumor size. Radiologic model and combined model exhibited equally diagnostic performance in the group with tumor size <50 mm. Combined model presented the significant diagnostic performance in the group with tumor size ≥50 mm (Table 4).

The proportion of Hepa-1 was significantly higher in true negative (TN) patients and false negative (FN) patients than in true positive (TP) patients (TN vs. TP: 29 [93.5%] vs. 16 [64%], P = 0.008, FN vs. TP: 10 [100%] vs. 16 [64%], P = 0.036). We did not found significant difference concerning the proportion of tumor necrosis among TP patients, TN patients, FN patients, FP patients (P = 0.061–1.0).

Table 3 Univariate and Multivariate Regression Analysis of cHCC-CCA Patients

Variable	Univariable Analysis	*P* value	Multivariable Analysis	*P* value
Clinical variable				
Age	1.014 (0.966–1.064)	0.567		
Gender	2.077 (0.618–6.985)	0.238		
Etiology				
None	Reference	0.301		
HBV	0.175 (0.019–1.589)	0.122		
HCV	0.200 (0.011–3.661)	0.278		
AFP	0.891 (0.347–2.288)	0.810		
CA19-9	4.580 (1.316–15.932)	0.017*		
ALT	1.003 (0.990–1.017)	0.625		
AST	1.006 (0.982–1.032)	0.613		
TBIL	1.018 (0.972–1.067)	0.454		
DBIL	1.022 (0.958–1.091)	0.506		
Albumin	1.044(0.937–1.163)	0.436		
GGT	1.003 (0.996–1.010)	0.435		
PT	0.700 (0.459–1.068)	0.098		
PLT	1.000 (0.993–1.006)	0.885		
Radiologic results				
Hypovascular component ≥50%	18.051 (4.597–70.876)	0.000*	10.873 (2.549–46.391)	0.001*
Tumor size	1.633 (0.957–2.787)	0.070		
Tumor margin	3.244 (1.219–8.629)	0.018*		
Internal arteries	1.122 (0.439–2.868)	0.811		
Major imaging features				
Non-rim like enhancment in AP (%)	0.195 (0.065–0.588)	0.004*		
Non-peripheral "washout"in PVP or DP/TP	0.195 (0.065–0.588)	0.004*		
Enhancing capsule	0.297 (0.103–0.859)	0.025*		
Ancillary imaging features				
Corona enhancement	1.333 (0.275–6.457)	0.721		
Non-enhancing capsule	NA	1.000		
Nodule-in-nodule	NA	1.000		
Mosaic architecture	0.844 (0.269–2.648)	0.771		
Blood products in mass	0.624 (0.16–2.436)	0.497		
Targetoid mass, imaging appearance				
Rim hyperenhancement in AP	6.353 (2.0–20.179)	0.002*		
Peripheral "washout" in PVP or DP/TP	4.043 (1.154–14.164)	0.029*		
Delayed central enhancement	20.632 (3.517–233.071)	0.002*	14.242(1.561–129.917)	0.019*
Biliary dilatation	4.387 (0.465–41.404)	0.197		
Lymph node invasion	3.187 (0.315–32.244)	0.326		
Liver capsular retraction	2.750 (0.496–15.246)	0.247		

Notes: Multivariate analysis with the Cox regression were used via backward LR stepwise selection. Data are reported as hazard ratios (95% CIs). *$P < 0.05$.
Abbreviations: cHCC- CCA, combined hepatocellular- cholangiocarcinoma; HBV, hepatitis B virus; HCV, hepatitis C virus; AFP, alpha-fetoprotein; CA19-9, carbohydrate antigen-199; ALT, alanine aminotransferase; AST, aspartate aminotrans ferase; TBIL, total bilirubin; DBIL, direct bilirubin; GGT, gamma-glutamyltransferase; PT, prothrombin time; PLT, platelet count; AP, arterial phase; PVP, portal vein phase; DP, delayed phase; TP, transitional phase.

Discussion

Our study demonstrated that radiologic model included quantitative assessment of hypovascular component and delayed enhancement could help differentiation cHCC-CCA from HCC. Regarding subgroup analyses, radiologic model remain good performance in LR-M group. Same as it in the tumor size <50 mm group. Combined model which added CA19-9 to radiologic model presented good performance in LR-4/5 group. Same as it in the tumor size ≥50 mm group. The current

Table 4 Diagnostic Performance for cHCC- CCA

Variable	AUC	95% CIs	Accuracy (%)	Sensitivity (%)	Specificity (%)	PPV (%)	NPV (%)	*P* value
LR-M category	0.743	0.624–0.862	72.86	62.86	85.71	81.48	69.77	0.000*
Radiologic Model	0.821	0.719–0.924	80	71.43	88.57	86.21	75.61	0.000*
CA19-9+Radiologic Model	0.838	0.741–0.936	80	71.43	88.57	86.21	75.61	0.000*
Tumor size <50mm								
Radiologic Model	0.866	0.746–0.986	87.76	76.19	96.43	84.38	94.12	0.000*
CA199+Radiologic Model	0.854	0.723–0.986	87.76	76.19	96.43	84.38	94.12	0.000*
Tumor size ≥50mm								
Radiologic Model	0.714	0.497–0.932	61.90	64.29	57.14	75.00	44.44	0.054
CA199+Radiologic Model	0.730	0.511–0.948	66.67	71.43	57.14	76.92	50.00	0.040*
LR-4/5								
Radiologic Model	0.633	0.413–0.853	79.49	30	96.55	75.00	80.00	0.273
CA199+Radiologic Model	0.717	0.508–0.927	82.05	50	93.10	71.43	84.36	0.042*
LR-M								
Radiologic Model	0.841	0.686–0.996	81.48	90.90	40.00	86.96	50.00	0.000*
CA199+Radiologic Model	0.859	0.703–1.015	81.48	90.90	40.00	86.96	50.00	0.000*

Note: *$P<0.05$.
Abbreviations: cHCC- CCA, combined hepatocellular- cholangiocarcinoma; CA 19–9, Carbohydrate antigen-199; AUC, area under the curve; CI, confidence interval.

histopathologic results indicated the complexity component of cHCC-CCA. We found the proportion of macrotrabecular appearance was significantly difference between cHCC-CCA and HCC.

Our results exhibited that radiologic model obtained good accuracy for the distinction cHCC from HCC (accuracy: 80%). Gigante et al reported that a mixed style of imaging appearance showed a 48% sensitivity and 81% specificity related to the diagnosis of cHCC-CCA.[10] The mixed style of imaging appearance included progressive enhancement of the entire lesion and arterial enhancement with washout, which is partly similar to us. This outcome is also in accordance with Sammon et al.[21] Lee et al reported that the combination of any three LR-M features presented accuracy of 80.8% for identification of cHCC-CCA from HCC,[11] which is comparable with us. But they found only targetoid appearance, biliary obstruction, and infiltrative margin were independent factors for the differentiation of cHCC-CCA and HCC. Liver surface retraction and mixed pattern did not relate to it. So their accuracy may be overestimated, which may be able to achieve equal accuracy with us by more imaging features. More factors in model may result to lower sensitivity and higher specificity than us (54.5% vs. 71.43, 93.9 vs. 88.57). Jiang et al demonstrated that diagnostic model including AFP, CA19-9, absence of "blood products in mass" showed AUC of 0.862, sensitivity of 76%, and specificity of 88% for M-CCs. M-CCs was defined as LR-M entities consisting of intrahepatic cholangiocarcinoma (iCCA) and cHCC-CCA. They only enrolled cHCC-CCA with LR-M features, which heterogeneity of tumor component may be lower than us.[13]

Our radiologic model also presented high PPV of differentiation cHCC-CCA from HCC (PPV: 86.21%). Patients with positive radiologic model were not suitable as a candidate for liver transplantation given 88.57% risk of cHCC-CCA. Though CA 19–9 was not an independent factor via multivariate regression, prior studies suggested CA 19–9 presented clinical value of identifying cHCC-CCA.[3] We found the combined model could improve specificity of cHCC-CCA in the LR-4/5 patients (specificity: 93.1%), biopsy for cHCC-CCA assessment may be obviated in those cases which may contribute to reduce potential risk by invasive operation. The sensitivity of the radiologic model for cHCC-CCA diagnosis was better than LR-M, but it was not as high as desired. The LR-M category is intended to trade-off sensitivity of the diagnosis of all malignant lesions, including iCCA, cHCC-CCA, and atypical HCC, which is required further distinction via biopsy.[10] To increase the sensitivity for distinguishing cHCC-CCA in LR-M patients, we performed subgroup analyses in LR-M patients. The results reported that radiologic model and combined model yielded equal performance with higher sensitivity concerning cHCC-CCA identification (both sensitivity: 90.9%).

Our radiologic model included ≥50% hypovascular component and delayed enhancement. Macrotrabecular appearance of cHCC-CCA was higher than HCC. As reported by previous studies, macrotrabecular-massive HCC could exhibit

imaging appearance with ≥50% hypovascular component. Moreover, tumor necrosis could be another reason for hypovascularity in AP. Tumor necrosis was frequently observed in larger tumor,[22] though the difference between two group of it was not significant (45.4% vs. 29.2%). Further, the subgroup analysis of radiologic model only showed significant distinction of cHCC-CCA in the group of tumor size <50mm not in the group of that ≥50mm. Tumor necrosis may contribute to the interfering with the diagnosis, at least in part. Interestingly, we did not found difference among TP patients, FP patients, TN patients, FN patients. Thus, the power of tumor necrosis required more studies. Well-differentiated HCCs may have insufficient development of the unpaired artery.[22–24] That may able to exhibit hypovascular invasion. We found the proportion of Hepa-1 was significantly higher in TN patients and FN patients than in TP patients. It provided some indication that the level of hepatocellular carcinoma component differentiation may impact the distinction of cHCC-CCA and HCC. Previous studies found imaging features of cHCC-CCAs were determined by a predominant pathological component, or HCC component correlated with LR-5 grade.[10,25,26] Those were partly consistent with our results. Delayed enhancement could derived from abundant fibrotic stroma which could also be another reason for hypovascluar in AP. The dominant histopathologic components of FN tumors in cHCC-CCA were HCC and intermediate cells component in current study. Researchers have postulated 3 different hypotheses of origin cell of cHCC-CCA:1. accompanying coexistence of HCC and iCCA in the same tumor; 2. malignant conversion of a hepatic progenitor cell; 3. dedifferentiation of an HCC or an iCCA.[27–29] Morphology of intermediate cells could locate an intermediate between a hepatocyte and a cholangiocyte.[2] Mixed morphological features of cHCC-CCA could lead to complicated findings of both HCC and iCCA. Further studies were required to proceed.

Several limitations to our study are that warrant mention. Firstly, our inclusion excluded patients diagnosed by pathological biopsy. This may attribute to a selection bias, for instance ignoring patients with unresectable tumor by biopsy diagnosis and losing aggressive imaging feature. However, the inclusion of pathological resection proven cHCC-CCA may have biased toward more patients like HCC, increasing our certainty that those characteristics would provide power in practice against the more classic cHCC-CCA. Secondly, it was a retrospective, single-center study, which holds the limited sample resulted from interventional treatment before surgery. The results should be validated in enlarged and multi-center studies in the future. Thirdly, it lacked the interpretation of hypovascular component by pathological mapping. The validation study is underway. Fourth, we excluded imaging features based on MRI during the multivariate regression analyses due to avoiding overfitting from the small sample.

The radiologic model, including ≥50% hypovascular component in AP and delayed enhancement, exhibited good performance of identifying the probability of cHCC-CCA from HCC. The proportion of macrotrabecular appearance was significantly difference between cHCC-CCA and HCC.

Funding

This work was supported by the National Natural Science Foundation of China (grant no. 61936013) and the Beijing Natural Science Foundation (7212051) and Beijing Excellent Talent Plan (2018000021469G290).

Disclosure

The authors report no conflicts of interest in this work.

References

1. Connell LC, Harding JJ, Shia J, et al. Combined intrahepatic cholangiocarcinoma and hepatocellular carcinoma. *Chin Clin Oncol*. 2016;5(5):66. doi:10.21037/cco.2016.10.02
2. Beaufrere A, Calderaro J, Paradis V. Combined hepatocellular-cholangiocarcinoma: an update. *J Hepatol*. 2021;74(5):1212–1224. doi:10.1016/j.jhep.2021.01.035
3. Brunt E, Aishima S, Clavien PA, et al. cHCC-CCA: consensus terminology for primary liver carcinomas with both hepatocytic and cholangiocytic differentation. *Hepatology*. 2018;68(1):113–126. doi:10.1002/hep.29789
4. Shetty AS, Fowler KJ, Brunt EM, et al. Combined hepatocellular-cholangiocarcinoma: what the radiologist needs to know about biphenotypic liver carcinoma. *Abdom Imaging*. 2014;39(2):310–322. doi:10.1007/s00261-013-0069-6
5. Santillan C, Chernyak V, Sirlin C. Li-rads categories: concepts, definitions, and criteria. *Abdom Radiol*. 2018;43(1):101–110. doi:10.1007/s00261-017-1334-x

6. Mitchell DG, Bruix J, Sherman M, et al. Li-rads (liver imaging reporting and data system): summary, discussion, and consensus of the li-rads management working group and future directions. *Hepatology*. 2015;61(3):1056–1065. doi:10.1002/hep.27304
7. Choi SH, Lee SS, Park SH, et al. Li-rads classification and prognosis of primary liver cancers at gadoxetic acid-enhanced MRI. *Radiology*. 2019;290(2):388–397. doi:10.1148/radiol.2018181290
8. Jeon SK, Joo I, Lee DH, et al. Combined hepatocellular cholangiocarcinoma: li-rads v2017 categorisation for differential diagnosis and prognostication on gadoxetic acid-enhanced MR imaging. *Eur Radiol*. 2019;29(1):373–382. doi:10.1007/s00330-018-5605-x
9. Marrero JA, Kulik LM, Sirlin CB, et al. Diagnosis, staging, and management of hepatocellular carcinoma: 2018 practice guidance by the American Association for the study of liver diseases. *Hepatology*. 2018;68:723–750. doi:10.1002/hep.29913
10. Gigante E, Ronot M, Bertin C, et al. Combining imaging and tumour biopsy improves the diagnosis of combined hepatocellular-cholangiocarcinoma. *Liver Int*. 2019;39(12):2386–2396. doi:10.1111/liv.14261
11. Lee HS, Kim MJ, An C. How to utilize lr-m features of the li-rads to improve the diagnosis of combined hepatocellular-cholangiocarcinoma on gadoxetate-enhanced MRI? *Eur Radiol*. 2019;29(5):2408–2416. doi:10.1007/s00330-018-5893-1
12. Zhou Y, Yin S, Zhao L, et al. CEUS and CT/MRI LI-RADS in association with serum biomarkers for differentiation of combined hepatocellular-cholangiocarcinoma from hepatocellular carcinoma. *Front Onco*. 2022;12:897090. doi:10.3389/fonc.2022.897090
13. Jiang H, Song B, Qin Y, et al. Diagnosis of LI-RADS M lesions on gadoxetate-enhanced MRI: identifying cholangiocarcinoma-containing tumor with serum markers and imaging features. *Eur Radiol*. 2021;31(6):3638–3648. doi:10.1007/s00330-020-07488-z
14. Shin J, Lee S, Hwang JA, et al. MRI-diagnosis of category LR-M observations in the liver imaging reporting and data system v2018: a systematic review and meta-analysis. *Eur Radiol*. 2022;32(5):3319–3326. doi:10.1007/s00330-021-08382-y
15. Rhee H, An C, Kim HY, et al. Hepatocellular carcinoma with irregular rim-like arterial phase hyperenhancement: more aggressive pathologic features. *Liver Cancer*. 2019;8(1):24–40. doi:10.1159/000488540
16. Cha H, Choi JY, Park YN, et al. Comparison of imaging findings of macrotrabecular-massive hepatocellular carcinoma using CT and gadoxetic acid-enhanced MRI. *Eur Radiol*. 2022;24. doi:10.1007/s00330-022-09105-7
17. Banerjee S, Wang DS, Kim HJ, et al. A computed tomography radiogenomic biomarker predicts microvascular invasion and clinical outcomes in hepatocellular carcinoma. *Hepatology*. 2015;62(3):792–800. doi:10.1002/hep.27877
18. An C, Kim DW, Park Y-N, et al. Single hepatocellular carcinoma: preoperative MR imaging to predict early recurrence after curative resection. *Radiology*. 2015;276(2):433–443. doi:10.1148/radiol.15142394
19. Sempoux C, Kakar S, Kondo F, et al. Combined hepatocellular-cholangiocarcinoma. In: Bosman FT, Carneiro F, Hruban RH, Theise ND, editors. *WHO Classification of Tumours: Digestive System Tumours*, 5th ed. Lyon: IARC; 2019:260–262.
20. Chernyak V, Fowler KJ, Kamaya A, et al. Sirlin, liver imaging reporting and data system (LI- RADS) version 2018: imaging of Hepatocellular Carcinoma In At-Risk Patients. *Radiology*. 2018;289:816–830. doi:10.1148/radiol.2018181494
21. Sammon J, Fischer S, Menezes R, et al. MRI features of combined hepatocellular- cholangiocarcinoma versus mass forming intrahepatic cholangiocarcinoma. *Cancer Imaging*. 2018;18(1):8. doi:10.1186/s40644-018-0142-z
22. Rhee H, Cho ES, Nahm JH, et al. Gadoxetic acid-enhanced MRI of macrotrabecular-massive hepatocellular carcinoma and its prognostic implications. *J Hepatol*. 2021;74(1):109–121. doi:10.1016/j.jhep.2020.08.013
23. Rhee H, Kim MJ, Park YN, et al. Gadoxetic acid-enhanced MRI findings of early hepatocellular carcinoma as defined by new histologic criteria. *J Magn Reson Imaging*. 2012;35(2):393–398. doi:10.1002/jmri.22828
24. Sano K, Ichikawa T, Motosugi U, et al. Imaging study of early hepatocellular carcinoma: usefulness of gadoxetic acid-enhanced MR imaging. *Radiology*. 2011;261(3):834–844. doi:10.1148/radiol.11101840
25. Choi SH, Jeon SK, Lee SS, et al. Radio-pathologic correlation of biphenotypic primary liver cancer (combined hepatocellular cholangiocarcinoma): changes in the 2019 who classification and impact on li-rads classification at liver MRI. *Eur Radiol*. 2021;31(12):9479–9488. doi:10.1007/s00330-021-07984-w
26. Li R, Yang D, Tang CL, et al. Combined hepatocellular carcinoma and cholangiocarcinoma (biphenotypic) tumors: clinical characteristics, imaging features of contrast-enhanced ultrasound and computed tomography. *BMC Cancer*. 2016;16:158. doi:10.1186/s12885-016-2156-x
27. Sia D, Villanueva A, Friedman SL, et al. Liver cancer cell of origin, molecular class, and effects on patient prognosis. *Gastroenterology*. 2017;152(4):745–761. doi:10.1053/j.gastro.2016.11.048
28. Tanimizu N, Nakamura Y, Ichinohe N, et al. Hepatic biliary epithelial cells acquire epithelial integrity but lose plasticity to differentiate into hepatocytes in vitro during development. *J Cell Sci*. 2013;126(Pt22):5239–5246. doi:10.1242/jcs.133082
29. Chen Y, Wong PP, Sjeklocha L, et al. Mature hepatocytes exhibit unexpected plasticity by direct dedifferentiation into liver progenitor cells in culture. *Hepatology*. 2012;55(2):563–574. doi:10.1002/hep.24712